



## Influence of operating parameters on performance of air-gap diffusion distillation device in desalination

Ping Wang, Lei Li, Lele Chen, Shiming Xu\*, Shuping Zhang, Lin Xu

*Key Laboratory of Ocean Energy Utilization and Energy Conservation of Ministry of Education, School of Energy and Power Engineering, Dalian University of Technology, Dalian 116024, China, Tel. +8613050539216; email: xsming@dlut.edu.cn (S. Xu), Tel. +8613050546586; email: wp2006@dlut.edu.cn (P. Wang), Tel. +8618041165581; email: lileistu@163.com (L. Li), Tel. +8618742509378; email: chen\_le@mail.dlut.edu.cn (L. Chen), Tel. +8618342245529; email: 2506033595@qq.com (S. Zhang), Tel. +8618641505707; email: linlin19872008@126.com (L. Xu)*

Received 19 December 2020; Accepted 6 May 2021

---

### ABSTRACT

Freshwater on the Earth is in short supply, and water resources are unevenly distributed. In order to solve the problem of water shortage, countries are striving to develop desalination technology. In this study, we described the calculation and experiment of the air-gap diffusion distillation (AGDD) in seawater desalination with MATLAB. The influence of the operating parameters was studied. The results showed that the inlet temperature of the hot liquid had a greater influence on the heat transfer coefficient than the cold liquid. Under the same conditions, the inlet temperature of the hot liquid increased 10°C, the local heat transfer coefficient increased 42.5%; but the inlet temperature of the cold liquid increased 10°C, the local heat transfer coefficient only increased 6%. And when the thickness and height of air-gap, inlet temperatures of cold and hot fluid, the mass flow rate of cold fluid were 5 mm, 0.9 m, 20°C, 65°C and 5 kg h<sup>-1</sup> respectively, the water production flux is up to 0.937 kg m<sup>-2</sup> h<sup>-1</sup>, and the water recovery rate is 3.37% which is much higher than similar research about air-gap membrane distillation. During the experiment, changes in operating parameters had no effect on the desalination rate of AGDD, and its desalination rate was higher than 99.8%.

*Keywords:* Air-gap diffusion distillation; Local heat transfer coefficient; Desalination

---

### 1. Introduction

The Earth is rich in water resources. 71% of the Earth's surface is covered with water resources. However, freshwater resources are extremely scarce and salt-water accounts for 94.47% of the water. For the remaining freshwater resources, long-term frozen freshwater resources such as polar ice and alpine glaciers account for 87%, and rivers, lakes, and shallow groundwater account for only 0.26% of the total freshwater. This part of the water is also water that human beings can actually use. In 1977, the UN-Water Conference proposed that water would soon become a

serious social crisis, and the next crisis after the oil crisis would be water [1].

In order to solve the problem of water shortage, countries are striving to develop desalination technology. In the 1950s, the United States, Japan, and Europe began to research and the industrial application of desalination, and desalination technology was raised to a strategic height to promote the development and application of this technology. By the end of 2017, more than 160 countries and regions around the world had utilized desalination technology, and nearly 20,000 desalinated plants had been built or were under construction. The total desalination capacity was about

---

\* Corresponding author.

104.32 million tons/d [2]. Desalination methods are mainly divided into three categories: heat treatment, membrane treatment, and chemical methods [3].

Membrane distillation (MD) is a combination of membrane separation technology and evaporation technology. According to the different methods of permeation to the cold side for condensation, MD is classified into four categories: direct contact membrane distillation (DCMD), air-gap membrane distillation (AGMD), vacuum membrane distillation (VMD) and sweeping gas membrane distillation (SGMD) [4,5]. Adham et al. [6] evaluated the feasibility of membrane distillation desalination and studied the performance of a membrane under different operating conditions. Unal et al. [7] used an experimental method to remove boron from geothermal water using AGMD. The study showed that high heat loss was one of the main factors affecting the application of the membrane distillation systems. Mengual et al. [8] studied VMD in a capillary membrane module and evaluated the heat transfer coefficients in both the lumen and the shell side of the membrane module by experience. Hogan et al. [9] used solar energy to heat seawater in the MD device, which could produce 50 kg of freshwater per day. Zakrzewska et al. [10] compared the effects of various separation methods for low-level radioactive wastewater. The results showed that the membrane separation had significant advantages. The MD had a very high rejection rate, and it could concentrate the radioactive wastewater in a small volume. Khayet et al. [11] developed a Monte Carlo (MC) simulation model to study heat and mass transfer through hydrophobic membranes applying DCMD process. This model was designed to be comprehensive in its approach. It can predict simultaneously the DCMD process vapor flux (permeability) and membrane surface temperatures, taking into consideration the effects of the applied membrane physical properties. Andrjesdóttir et al. [12] compared the experimental results of DCMD with deionized water and aqueous salt solutions of NaCl with concentration levels of up to 15 ppm as feed to study heat and mass transfer in DCMD, and found that a decrease in permeate flux with increasing salinity, and an increase in permeate yield was observed for higher feed temperatures. Huang et al. [13] studied the conjugate heat and mass transfer of SGMD in a hollow fiber membrane tube bank with an in-line arrangement, and they investigated the influences of various longitudinal and transverse pitch-to-diameter ratios on the conjugate heat and mass transfer. Cong et al. [14] used the surface-modified multi-layer porous ceramic tubes as microporous hydrophobic membrane to applied in membrane distillation. They found that the modified porous ceramic tubes were successfully applied in MD with a lab-scale AGMD system, the salt rejection rates of all the tests were <99.9% with over 16 h of continuous running. Cheng et al. [15] proposed a design of counter-current AGMD of the hollow fiber module (AGMD-HF) to improve the permeate flux and to keep the advantage of the high thermal efficiency in air-gap membrane distillation (AGMD) for desalination when the velocity of cold solution side and hot tube side is  $2 \text{ L min}^{-1}$ , the temperature of cold solution side is  $20^\circ\text{C}$ , the temperature of hot tube side is  $60^\circ\text{C}$ , packing

density is 0.6, air/vapor gap kinematic viscosity is  $0.2 \text{ mm}^2 \text{ s}^{-1}$ , the mass vapor flux is  $3.5 \text{ kg m}^{-2} \text{ h}^{-1}$ . Singh et al. [16] studied desalination by AGMD using a two hollow-fiber-set membrane module, in their study, when the hot brine inlet temperature varying between  $70^\circ\text{C}$  and  $94^\circ\text{C}$ , and the inlet hot brine pressure goes up to 138 kPa. The hot brine flow rate was  $75 \text{ mL min}^{-1}$ . The cooling water was introduced at  $20^\circ\text{C}$  in all cases at a flow rate of  $150 \text{ mL min}^{-1}$ . The highest water vapor flux is around  $28 \text{ kg m}^{-2} \text{ h}^{-1}$ .

MD distillation has the advantages of high separation efficiency, mild operating conditions, and low requirements on the mechanical strength of the membrane. Compared to other membrane distillation, AGMD has the following advantages: (1) The structure is simple, operating under normal pressure; (2) The existence of air-gap reduces heat loss, and well weakens the temperature polarization effect and improves thermal efficiency; (3) It has high technical adaptability, few restrictions, flexible and simple operation. However the preparation of membranes is complex, expensive, and requires regular cleaning. So in order to adopt the advantages of AGMD and avoid the disadvantages caused by the existence of the membrane, the air-gap diffusion distillation (AGDD) was proposed.

AGDD studied in this paper has similarity with the AGMD. In the AGDD model, we canceled the hydrophobic membrane from the AGMD, and the hot channel was filled with a highly hydrophilic porous medium. Because the water in the porous medium is not saturated, the water cannot overflow through the porous medium into the air-gap, which was proved by that the desalination rate of all experiments is higher than 99.8%. The presence of the porous media reduced the mass transfer resistance in diffusion. The porous medium increases the effective diffusion area and enhances the disturbance of the hot liquid so that the mainstream of the fluid and the boundary layer can exchange heat fully and increases freshwater production. What's more, the AGDD could use low-grade heat as an external heat source to reduce energy consumption.

## 2. Physical model of AGDD

As shown in Fig. 1, the cold fluid flowed into the cold channel from the bottom of the condenser and then flowed out from the top of the condenser. The fluid was heated by the external heat source, then the fluid flowed in the hot channel (the hot channel is precisely the porous medium) from the top of the evaporator and then flowed out from the bottom of the evaporator. When the device was running, the water vapor evaporated at the interface between the porous layer of the hot channel and the air-gap, and then diffused in the air-gap. When the water vapor touched the cold plate, the vapor released the heat and condensed on the cold plate, and the condensed water flowed down the condensing plate due to the action of gravity. Then freshwater was collected under the bottom of the device. The device operated at atmospheric pressure, and it was insulated from the external environment by wrapping the insulation layer outside the device. The hot fluid and cold fluid flows in the channel went in different directions. The hot channel was covered with a highly hydrophilic porous medium.

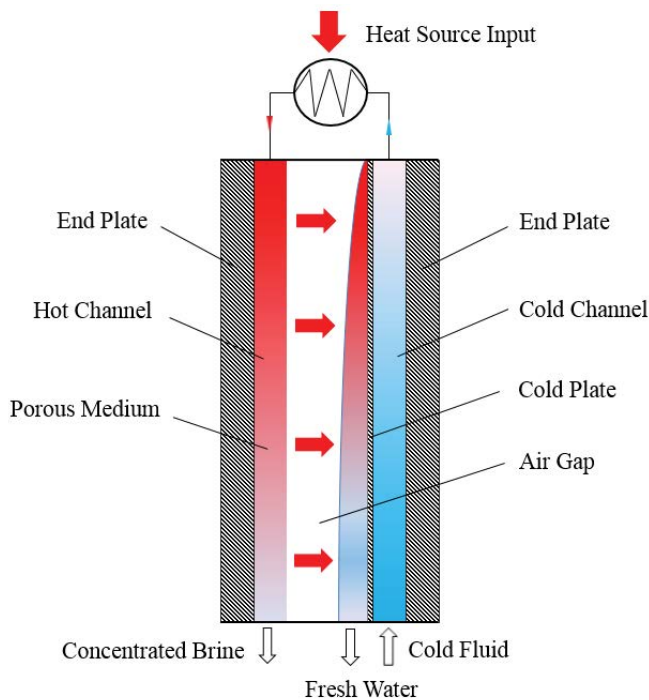


Fig. 1. Physical model of AGDD in seawater desalination.

### 3. Heat and mass transfer analysis of AGDD in seawater desalination

The AGDD in the seawater desalination device was composed of two parallel plates, a porous sponge, an air-gap layer, and a cold fluid flow channel. In order to analyze the heat and mass transfer in the device better, the following assumptions were made for the mathematical model of AGDD in seawater desalination [17]:

- The device had no heat exchange with the outside environment. Thus, the device did not have heat loss.
- The system was running in a steady state.
- The cold fluid and the hot liquid flowed in the channel only in the  $x$ -direction.
- The natural convection and the radiation in the air-gap were ignored, and it was considered that the only heat exchange in the air-gap was heat conduction in the  $y$ -axis direction.
- The surface of the porous medium was infiltrated, and the liquid film on the surface of the porous medium was ignored.

As shown in Fig. 2, the micro-element method was used for the analysis.

#### 3.1. Heat passing through the hot channel

The hot channel was filled with a porous medium, and the hot fluid flowed in the porous medium. When the device was running in a steady-state, the porous medium was infiltrated with seawater, the flow of the hot fluid in the hot runner was slow, and the heat exchange mode in the

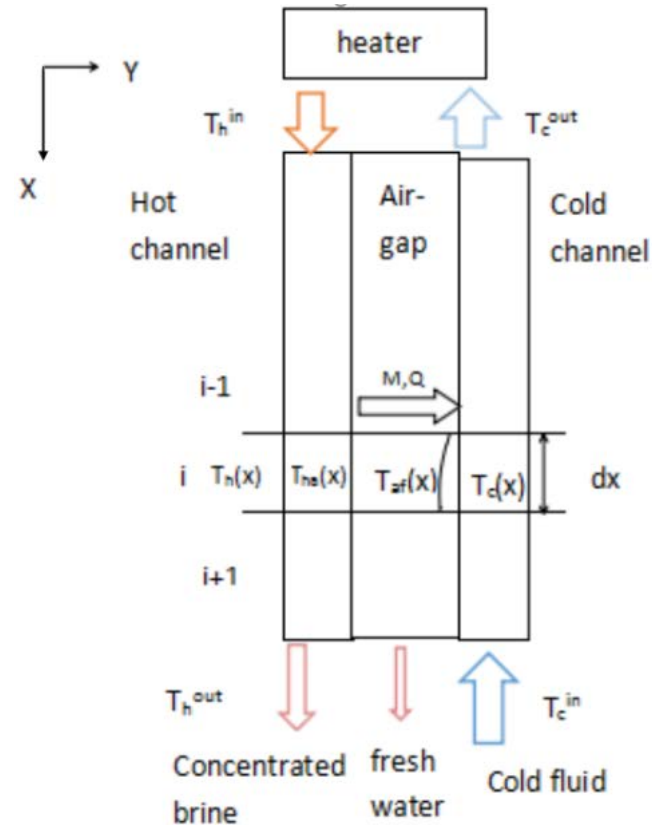


Fig. 2. Mathematical model of the AGDD in seawater desalination.

hot runner could be regarded as conduction. The heat flux calculation formula [18]:

$$q_h(x) = \frac{k_c \times (T_h(x) - T_{ha}(x))}{b} \quad (1)$$

where  $k_c$  is the thermal conductivity in the hot channel ( $\text{W m}^{-1} \text{K}^{-1}$ ), seen in [19,20];  $T_h$  is the temperature of seawater (K);  $T_{ha}$  is the temperature of the water vapor in the interface of the hot channel and the air-gap (K);  $b$  is hot channel width (m).

#### 3.2. Heat passing through the air-gap

There were three heat exchange methods in the air-gap layer, including conduction, natural convection, and radiation. Since the vapor was diffused in the air-gap, the natural convection and radiation in the air-gap were weak, and they could be ignored. The hot liquid evaporated in the interface between the porous medium and the air-gap. The vapor diffused in the air-gap and released heat on the cold plate. The heat passing through the air-gap ( $q_a$ ) could be divided into two parts. One type of heat, the latent heat of vaporization, was taken by the water vaporization process, and the other heat is transferred through the air-gap by conduction. Since the thickness of the liquid film was much thinner than the thickness of the air-gap, it could be negligible.

The formula of heat passing through the air-gap could be simplified as follows:

$$q_a(x) = J_v(x) \times \gamma + k_a \frac{T_{ha} - T_{af}}{\delta_a} \quad (2)$$

where  $J_v$  is the diffusion flux of water vapor in air-gas ( $\text{kg m}^2 \text{s}^{-1}$ ),  $\gamma$  is latent heat of water evaporation ( $\text{J kg}^{-1}$ );  $k_a$  is thermal conductivity of air-gap ( $\text{W m}^{-1} \text{K}^{-1}$ );  $T_{af}$  is the temperature of condensate film (K);  $\delta_a$  is thickness of air-gap (m).

### 3.3. Diffusion flux in the air-gap

When the device was running steadily, on the surface of the porous medium, the vapor evaporated continuously and diffused from the hot side to the cold side, driven by the pressure difference of the vapor. The diffusion flux could be calculated by the following formula [17]:

$$J_v(x) = \frac{D_{AB}(x)M_v}{\delta_a R T_{ave}(x)} (P_{ha,sw}(x) - P_{af,sw}(x)) \quad (3)$$

where  $D_{AB}$  is diffusion coefficient of water vapor in air ( $\text{m}^2 \text{s}^{-1}$ );  $P_{ha,sw}$  is the partial pressure of the water vapor in the interface of the hot channel and the air-gap (Pa), and  $P_{af,sw}$  is the partial pressure of the water vapor in the condensate film (Pa), seen in [21,22];  $R$  is universal gas constant ( $\text{J mol}^{-1} \text{K}^{-1}$ );  $T_{ave}$  is the average temperature from the interface of the hot channel and the air-gap to the condensate film (K).

### 3.4. Heat passing through the liquid film

The vapor released the heat and condensed on the surface of the cooling plate. The condensed freshwater flowed down under the action of gravity, and it was collected at the bottom of the device according to the law of mass conservation. The freshwater production of the device could be obtained with the following formula:

$$m_f(x) = \int_0^{l_b} J_v(x) B dx \quad (4)$$

where  $B$  is hot channel thickness (m).

### 3.5. Heat passing through the cold channel

The heat of the condensate film passed through the cold plate to the cold channel. The method of the heat transfer in the cold plate was heat conduction. The heat flux of the cold plate could be calculated by the following formula:

$$q_{cw}(x) = \frac{k_{cw} (T_{fp}(x) - T_{pc}(x))}{\delta_{cw}} \quad (5)$$

where  $k_{cw}$  is thermal conductivity of cooling plate ( $\text{W m}^{-1} \text{K}^{-1}$ );  $\delta_{cw}$  is thickness of cooling plate (m);  $T_{fp}$  is the

temperature between the cold plate and the condensate film (K);  $T_{pc}$  is the temperature between the cold plate and cold channel (K).

The heat passing through the cold plate was absorbed by the seawater in the cold channel:

$$q_c(x) = h_c (T_{pc}(x) - T_c(x)) \quad (6)$$

where  $h_c$  is convective heat transfer coefficient of the cold channel ( $\text{W m}^{-2} \text{K}^{-1}$ ), it could be obtained by the following formula [23];  $T_c$  is the temperature of the cold channel (K).

### 3.6. Quantity of heat from the external heat source

The cold fluid flowed out from the top of the condenser and it was heated by and external heat source. The hot fluid flowed into the hot channel from the top of the evaporator. The quantity of heat provided by the external heat source could be calculated by the following formula:

$$Q_{heat} = m_c (H_h^{in} - H_c^{out}) \quad (7)$$

where  $m_c$  is mass flow rate of cold fluid ( $\text{kg h}^{-1}$ );  $H_h^{in}$  is the enthalpy of heat fluid inlet ( $\text{J kg}^{-1}$ );  $H_c^{out}$  is the enthalpy of cold fluid outlet ( $\text{J kg}^{-1}$ ).

The local heat transfer coefficient in the interface of the hot channel and the air-gap is as follows [24]:

$$h_{tx}(x) = \frac{q_a(x)}{T_{ha} - T_c} \quad (8)$$

The average heat transfer coefficient is in the interface of the hot channel and the air-gap as follows:

$$h_{tm}(x) = \frac{\int_0^l h_{tx}(x) dx}{L} \quad (9)$$

where  $L$  is air-gap height (m).

## 4. Experiment for the AGDD in the seawater desalination

### 4.1. Experimental system

The schematic diagram of set-up and the photograph of the actual set-up of AGDD in the seawater desalination test bench is shown in Fig. 3. The heat source was provided by an electric heating rod, and the heat of the electric heating rod was controlled by the transformer and the regulated power source, which could change the inlet temperature of the hot fluid. By adjusting the valve of the pump to control the mass flow rate of the fluid, and the thickness of the air-gap layer was controlled by increasing or decreasing the air-gap layer frame. The temperature of the fluid in the cryogenic flume was controlled in order to control the inlet temperature of the cold fluid. The experimental distillation apparatus and the outer surface of the pipeline were covered with a thermal insulation sponge to reduce the heat loss. A measuring cylinder was placed at the bottom of the

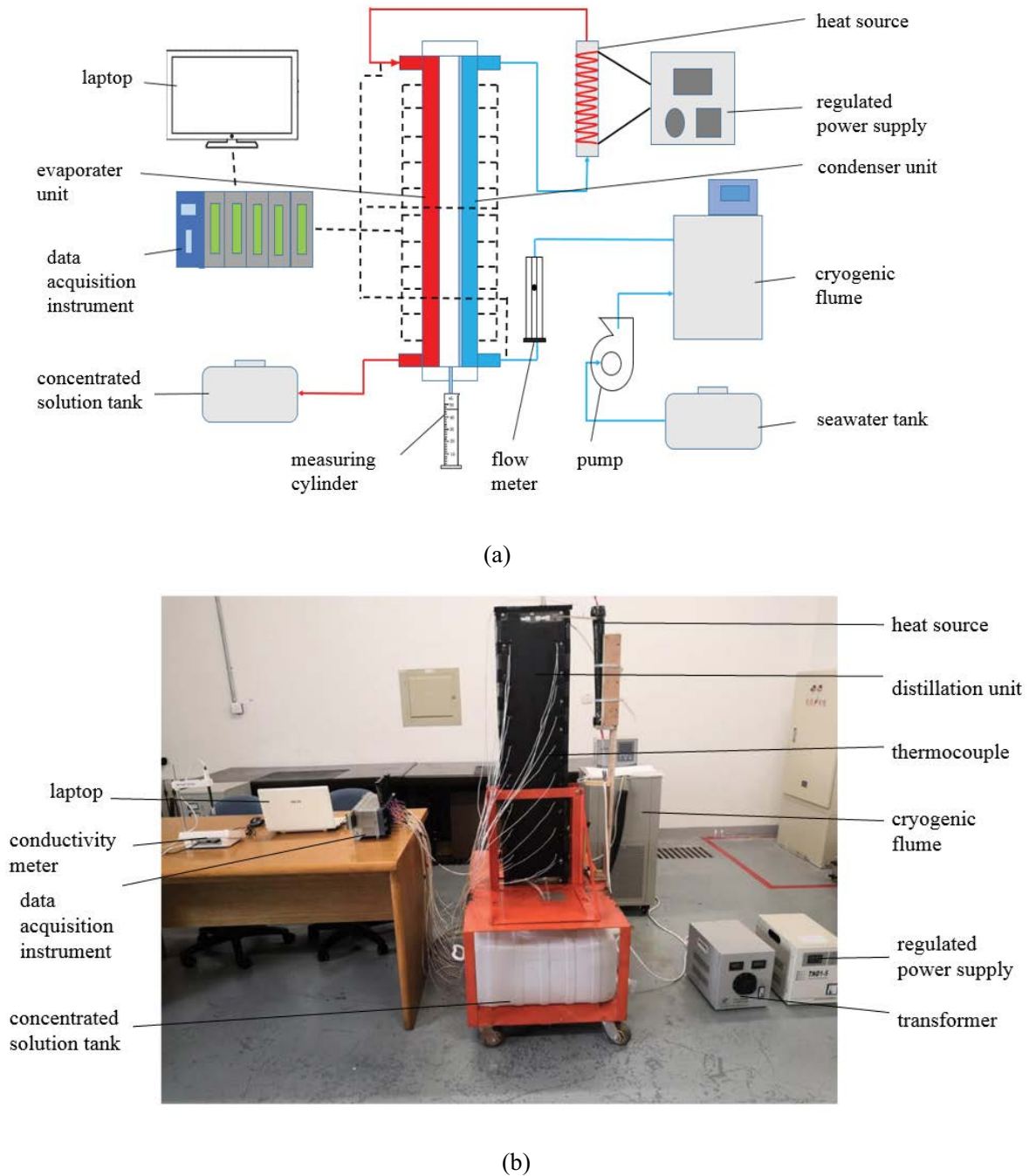


Fig. 3. Diagram of the AGDD seawater desalination experiment: (a) Schematic diagram of the AGDD set-up and (b) photograph of the actual set-up.

freshwater outlet of the air-gap layer to collect freshwater. The structure parameters and materials of the device are listed in Table 1.

#### 4.2. Experimental procedures

The main research purpose of this paper is to explore the influence of operating parameters on performance of the AGDD. The feed solution used in the experiment is NaCl aqueous with 3.5 wt.%. During experiment

procedure, the feed solution enters the condenser unit through the pump, and through the flow meter and cryogenic flume to control mass fluid rate and inlet temperature of the cold fluid separately to meet the requirements. The cold fluid flows through the condenser from the bottom up absorbs the condensation heat of water vapor, and then it is heated again by the heat resource. The inlet temperature of the hot fluid is controlled by the heat of the electric heating rod. And then the hot fluid flows through the hot channel (porous media) from top to bottom under

the action of gravity, at the same time, part of the fluid evaporates to produce water vapor, the vapor diffuses through air-gap to the condensation plate and condenses on it to become freshwater and release latent heat. At last, the freshwater flows from the bottom of the device and is collected by a measuring cylinder, the concentrated solution in the hot channel flows into the water tank.

The temperature is measured by thermal resistance, and display on the computer through the data acquisition instrument.

After the device runs stably (the parameters are basically unchanged), the data acquisition system starts to record, and the measuring cylinder starts to collect and produce freshwater. Each experiment runs for half an hour as a group. After 30 min, the data acquisition system automatically saves the temperature data measured by the

thermal resistance, and uses an electronic scale to measure the quality of the water collected in the measuring cylinder. Each group of experiments is repeated three times, and the average value was taken at the end.

The equipment and measuring instruments involved in the experiment are shown in Table 2.

#### 4.3. Porous media

Porous media used in the AGDD is polyvinyl alcohol (PVA) sponge, its main chemical composition is polyvinyl alcohol. It has strong hydrophilicity and will not denature at high temperature. The pore size of the PVA sponge used in this article is about 100 microns. Fig. 4 is the physical image and electron microscope image of the sponge respectively.

The concept of uncertainty was different with the measurement error. There are many factors that affect the uncertainty of an experiment. The experimental environment and experimental equipment will have a strong or weak influence on the test results of the experiment.

The uncertainty of the experimental measurement was calculated, and the maximal combined standard uncertainty can be obtained under the given conditions [24] and results are listed in Table 3.

### 5. Analysis of the research results

The method of controlling variables was used to study the effects of the cold fluid inlet temperature, hot fluid inlet temperature, mass flow rate, air-gap thickness and air-gap

Table 1  
Structure parameters and materials of the device

Item	Material	Thickness (mm)	Length (mm)	Height (mm)
End plate	PMMA: Polymethyl methacrylate	25	240	1,100
Porous medium	PVA sponge	5	200	900
Air-gap	/	5	200	900
Cold plate	SUS 316L	1	240	1,100

Table 2  
Equipment and measuring instruments involved in the experiment

Item	Type	Accuracy	Measuring range
Thermal resistance	WPZ PT100 (three-wire)	$\pm(0.15 + 0.002  t )$ °C	-70°C~500°C
Flow meter	Glass rotameter LZB-4	2.50%	10–100 mL h <sup>-1</sup>
Data acquisition instrument	IM MX100	/	/
Pump	WS246	/	20 L min <sup>-1</sup>
Electronic scale	Hochoice	0.5 g	0–2,000 g
Cryogenic flume	AC5600B	$\pm 0.05$ °C	5°C~100°C

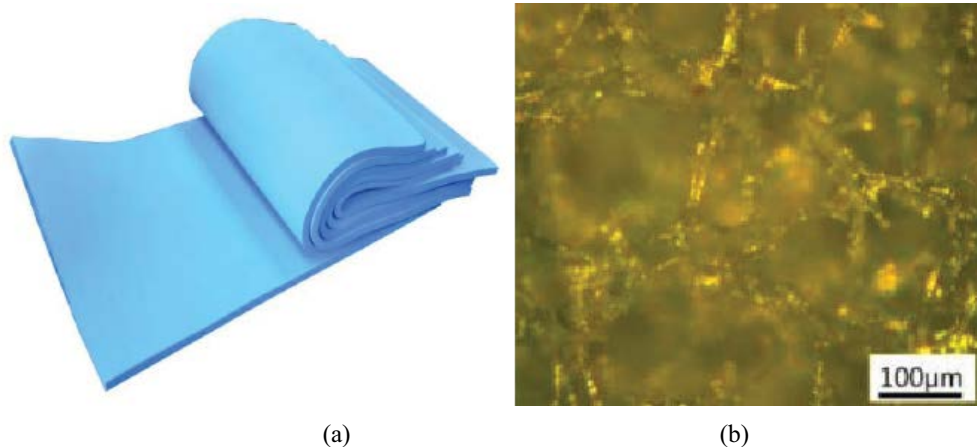


Fig. 4. (a) Physical image and (b) electron microscope image of the sponge.

Table 3  
Calculation of the maximal combined standard uncertainty

Parameters	Symbol	Measuring range	Maximal combined standard uncertainty
Inlet temperature of the hot fluid	$t_h^{\text{in}}$	50.0°C~65.0°C	0.45°C
Inlet temperature of the cold fluid	$t_c^{\text{in}}$	20.0°C~30.0°C	0.37°C
Mass flow rate	$m_c^{\text{in}}$	2.0~5.0 L h <sup>-1</sup>	0.16 L h <sup>-1</sup>

height. The program calculation results were compared with the experimental results, which could prove the trustworthiness of the program calculation. The grid was divided in the  $x$ -direction, the size of the grid was 0.01 m, and the heat transfer coefficient in each grid area was calculated in MATLAB. A scatter plot was drawn with the obtained data.

### 5.1. Influence of the hot fluid inlet temperature

When the inlet temperatures of the hot liquid were 50°C and 65°C, the temperature distribution of the hot channel and the cold channel in the  $x$ -direction was as shown in Fig. 5. The deviation between the calculation results and the experimental results was only 0.579°C, the deviation was small, and the trend of the change was consistent. With the increase of  $x$ , the temperatures of the hot and cold flow channels decreased. As shown in Fig. 5, when  $t_h^{\text{in}} = 65^\circ\text{C}$ , the slope of the temperature was larger in the  $x$ -direction, and the temperature difference between the hot channel and cold channels was larger. After calculating the data, we found that when the inlet temperature of the hot liquid was 50°C the temperature difference between the cold and the hot channels was about 9.1°C. When the inlet temperature of the hot liquid was 55°C, the temperature difference between the hot and cold flow channels was about 10.6°C. When the inlet temperature of the hot liquid was 60°C, the temperature difference was about 11.2°C, and when the inlet temperature of the hot liquid was 65°C, the temperature difference between the hot and cold channels was about 12.3°C. When the inlet temperature of the hot fluid was raised from 50°C to 65°C, the temperature difference between the hot and cold flow channels increased, the driving force of water vapor diffusion in the air-gap increased, and the freshwater production increased from 0.02676 to 0.11369 kg h<sup>-1</sup>, which was an increase of 100.3%.  $Q_{\text{heat}}$  increased by 31.1%, according to the formula of the gained output ratio (GOR) [25]:

$$\text{GOR} = \frac{m_f}{m_a} \quad (10)$$

$$m_a = \frac{Q_{\text{heat}}}{\gamma} \quad (11)$$

where  $\gamma$  is the latent heat of vaporization, it can be taken as 2326 kJ kg<sup>-1</sup> [26];  $m_a$  is the amount of water vapor consumed by the external heat source (kg s<sup>-1</sup>);  $m_f$  is freshwater productive rate (kg s<sup>-1</sup>).

By comparing Figs. 5 and 6, it can be seen that with the increase of  $t_h^{\text{in}}$ , the average temperature of the distillation

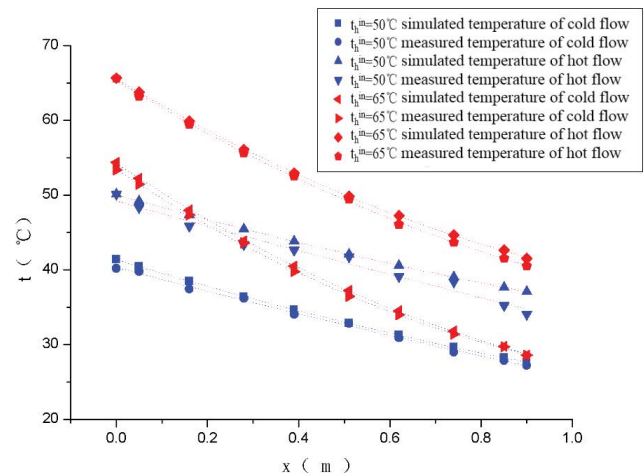


Fig. 5. Temperature distribution of the cold and hot fluid. ( $t_c^{\text{in}} = 30^\circ\text{C}$ ;  $\delta = 8$  mm;  $m_c^{\text{in}} = 3$  kg h<sup>-1</sup>;  $L = 0.9$  m).

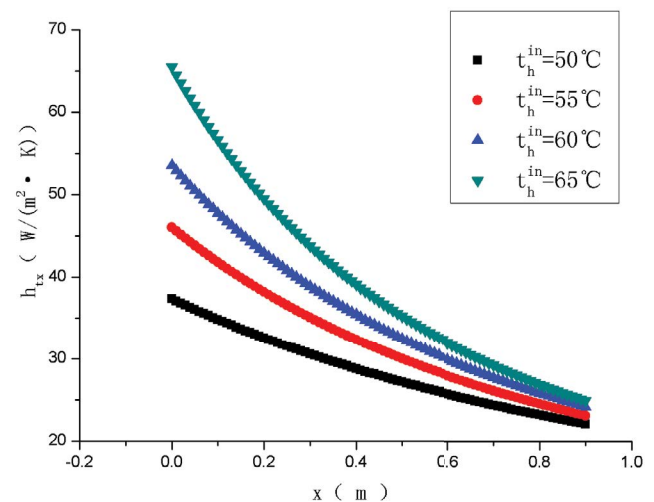


Fig. 6. Effect of the hot fluid inlet temperature on the local heat transfer coefficient ( $t_c^{\text{in}} = 30^\circ\text{C}$ ;  $\delta = 8$  mm;  $m_c^{\text{in}} = 3$  kg h<sup>-1</sup>;  $L = 0.9$  m).

unit increased, the local heat transfer coefficient increased, and the slope of the heat transfer coefficient was larger in the  $x$ -direction. This rule was consistent with the temperature in the  $x$ -direction. The increase of  $m_f$  was faster. Therefore, the GOR increased, and the deviations between the calculated results and the experimental values of  $m_f$  and GOR were 5.37% and 6.29%, respectively. The data could be plotted as shown in Figs. 7 and 8.

5.2. Influence of the cold fluid inlet temperature

When the inlet temperature of the cold fluid was 20°C or 30°C, the temperature distribution in the  $x$ -direction was as shown in Fig. 9. The deviation between the calculation results and the experimental results was only 0.757°C and the trend was consistent. When  $t_c^{in} = 20^\circ\text{C}$ , the slope of the temperature and the local heat transfer coefficient was larger in the  $x$ -direction, and the temperature difference between the hot channel and the cold channel was larger. When  $t_c^{in} = 20^\circ\text{C}$ , the temperature difference between the cold liquid and the hot liquid was about 12.7°C. When  $t_c^{in} = 25^\circ\text{C}$ , the temperature difference was about 10.6°C. When  $t_c^{in} = 30^\circ\text{C}$ , the temperature difference was about 8.2°C. By comparing Figs. 9 and 10, with the increase of  $t_c^{in}$ , the average temperature of the distillation unit increased, the local heat transfer coefficient increased, and the slope of the heat transfer coefficient was smaller in the  $x$ -direction. This rule was consistent with the temperature in the  $x$ -direction.

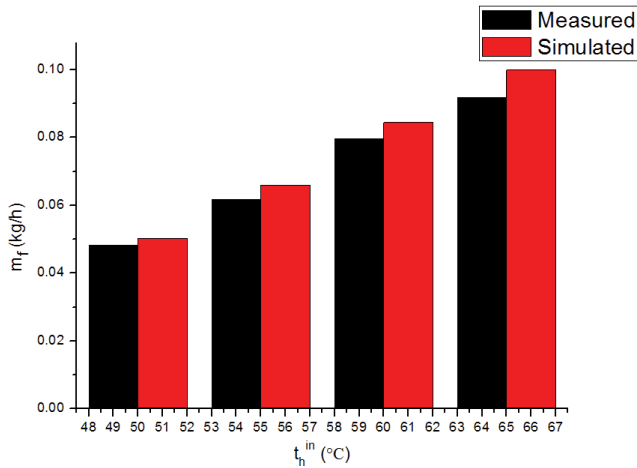


Fig. 7. Effect of the inlet temperature of the hot fluid on the fresh-water production ( $t_c^{in} = 30^\circ\text{C}$ ;  $\delta = 8\text{ mm}$ ;  $m_c^{in} = 3\text{ kg h}^{-1}$ ;  $L = 0.9\text{ m}$ ).

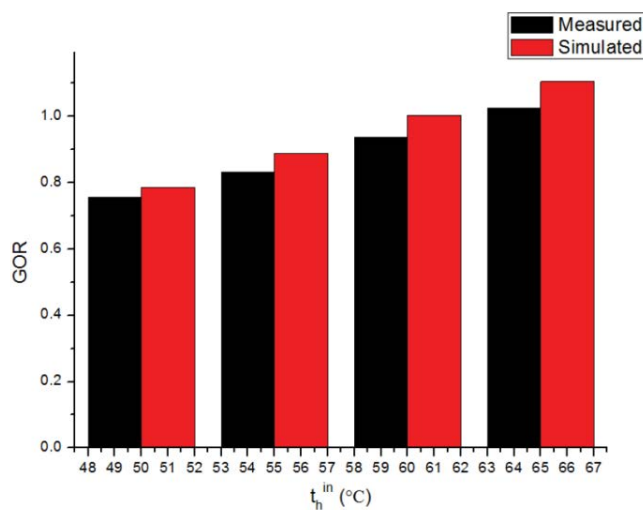


Fig. 8. Effect of the inlet temperature of the hot fluid on the GOR ( $t_c^{in} = 30^\circ\text{C}$ ;  $\delta = 8\text{ mm}$ ;  $m_c^{in} = 3\text{ kg h}^{-1}$ ;  $L = 0.9\text{ m}$ ).

When the temperature difference decreased, the driving force of the water vapor in the air-gap became weaker,  $m_f$  was reduced by 21.5%, and  $Q_{\text{heat}}$  was reduced by 35.7%. According to the formula of the GOR, the GOR rose. The deviations between the calculated and experimental values of  $m_f$  and GOR were 5.7% and 2.8%, respectively. The data could be plotted as shown in Figs. 11 and 12.

5.3. Influence of the mass flow rate

When the mass flow rate of the cold fluid was 2 or 5  $\text{kg h}^{-1}$ , the temperature distribution of the cold and hot flow channels was as shown in Fig. 13. The deviation between the calculation results and the experimental results was only 0.5°C and the trend was consistent. As can be seen from the graph, the temperatures of the hot and cold channels decreased with the  $x$ -increases. When the mass flow rate was 2  $\text{kg h}^{-1}$ , the slope of the temperature was smaller in the  $x$ -direction. The temperature difference

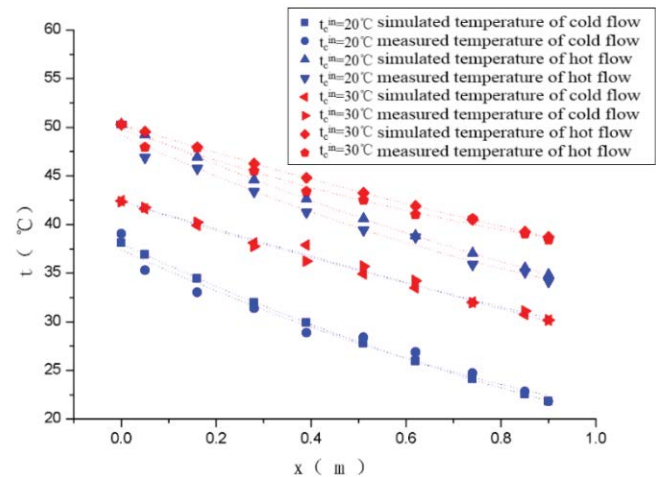


Fig. 9. Temperature distribution of the cold and hot fluid ( $t_h^{in} = 50^\circ\text{C}$ ;  $\delta = 8\text{ mm}$ ;  $m_c^{in} = 2\text{ kg h}^{-1}$ ;  $L = 0.9\text{ m}$ ).

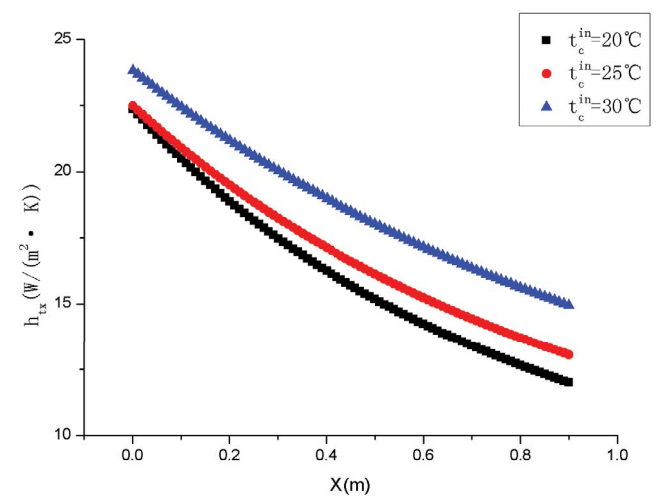


Fig. 10. Effect of the cold fluid inlet temperature on the local heat transfer coefficient ( $t_h^{in} = 50^\circ\text{C}$ ;  $\delta = 8\text{ mm}$ ;  $m_c^{in} = 2\text{ kg h}^{-1}$ ;  $L = 0.9\text{ m}$ ).

between the hot and cold channel increased with the increase of the mass flow rate. When the mass flow rate was 2 kg h<sup>-1</sup>, the temperature difference between the hot and the cold liquids was about 8.2°C. When the mass flow rate was 3 kg h<sup>-1</sup>, the temperature difference between the hot and the cold liquid was about 10°C. When the mass flow rate was 4 kg h<sup>-1</sup>, the temperature difference was about 11.4°C. When the mass flow rate was 5 kg h<sup>-1</sup>, the temperature difference was about 12.3°C, the diffusion driving force of the water vapor in the air-gap increased with the increase of the temperature difference.

As shown in Fig. 14, with the increase of the  $m_c^{in}$ , the slope of the local heat transfer coefficient was smaller in the  $x$ -direction. This rule was consistent with the temperature in the  $x$ -direction. And when the mass flow rate below 2.5 kg h<sup>-1</sup>, the larger the mass flow rate, the smaller the local

heat transfer coefficient. However; when the mass flow rate more than 2.5 kg h<sup>-1</sup>, the result is exactly the opposite, the larger the mass flow rate, the larger the local heat transfer coefficient. As shown in Fig. 15, the average heat transfer coefficient in the  $x$ -direction increased with the increase of the mass flow rate, when the mass flow rate increased from 2 to 9 kg h<sup>-1</sup>, the average heat transfer coefficient increased by 8.18%.

The results also explained the phenomenon that water production increases as the mass flow rate increases and GOR decreases as the mass flow rate increases, it could be shown in Figs. 16 and 17. When the mass flow rate increased from 2 to 5 kg h<sup>-1</sup>,  $m_f$  increases from 0.0317 to 0.0448 kg h<sup>-1</sup>, which was an increase of 41.3%. At the same time, the amount of external heat exchange required also increased.  $Q_{heat}$  increased from 17.45 W to 65.36 W, an increase of 274.56%, which was larger than the increase

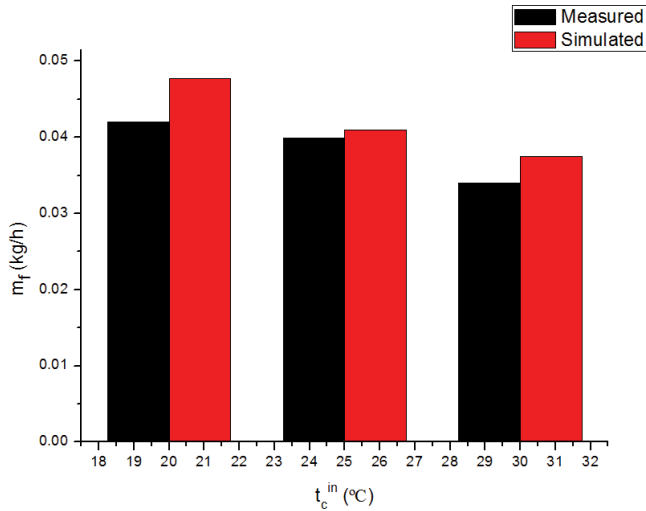


Fig. 11. Effect of the inlet temperature of the cold fluid on the freshwater production ( $t_h^{in} = 50^\circ\text{C}$ ;  $\delta = 8$  mm;  $m_c^{in} = 2$  kg h<sup>-1</sup>;  $L = 0.9$  m).

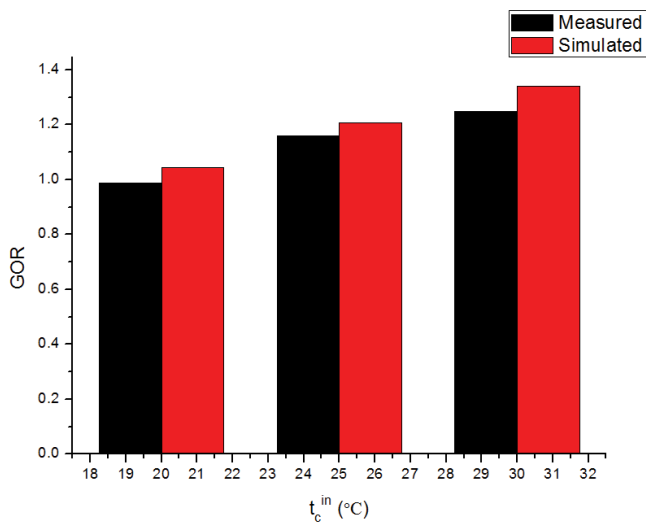


Fig. 12. Effect of the inlet temperature of the cold fluid on the GOR ( $t_h^{in} = 50^\circ\text{C}$ ;  $\delta = 8$  mm;  $m_c^{in} = 2$  kg h<sup>-1</sup>;  $L = 0.9$  m).

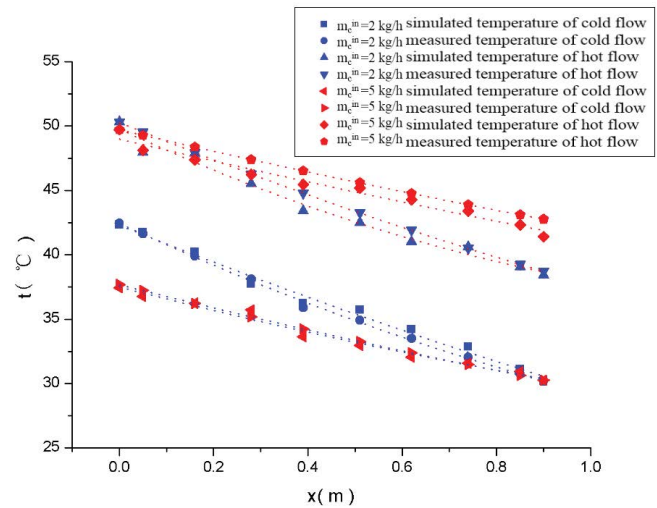


Fig. 13. Temperature distribution of the cold and hot fluid ( $t_h^{in} = 50^\circ\text{C}$ ;  $t_c^{in} = 20^\circ\text{C}$ ;  $\delta = 8$  mm;  $L = 0.9$  m).

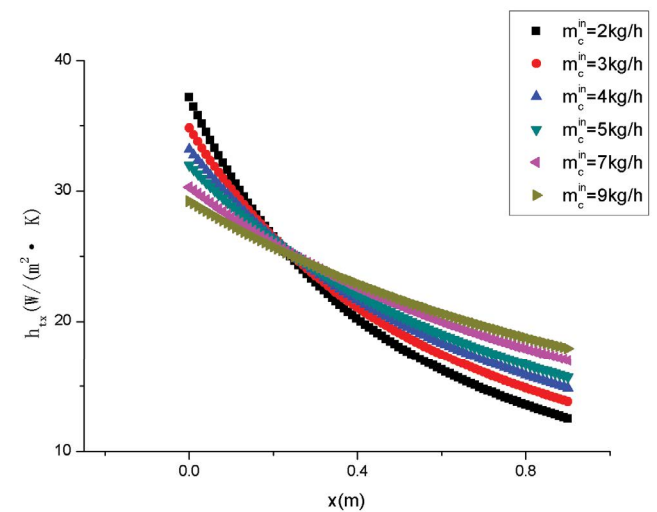


Fig. 14. Effect of the mass flow rate on the local heat transfer coefficient ( $t_h^{in} = 50^\circ\text{C}$ ;  $t_c^{in} = 20^\circ\text{C}$ ;  $\delta = 8$  mm;  $L = 0.9$  m).

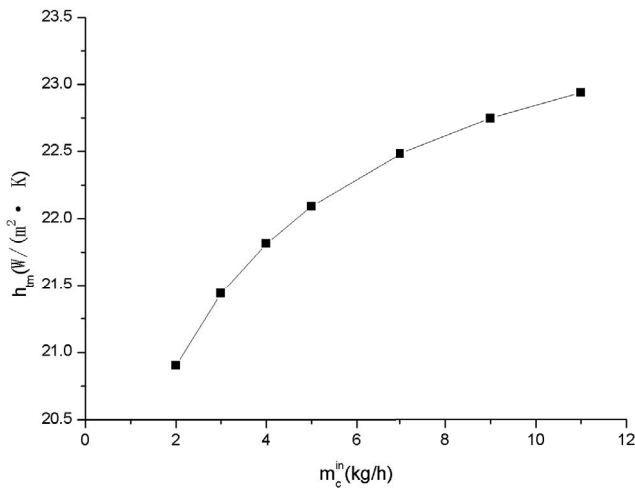


Fig. 15. Effect of the mass flow rate on the average heat transfer coefficient ( $t_h^{in} = 50^\circ\text{C}$ ;  $t_c^{in} = 20^\circ\text{C}$ ;  $\delta = 8$  mm;  $L = 0.9$  m).

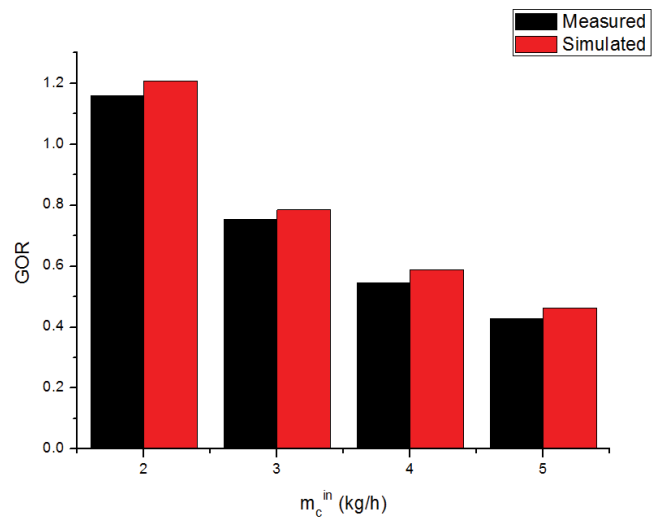


Fig. 17. Effect of the mass flow rate on the GOR ( $t_h^{in} = 50^\circ\text{C}$ ;  $t_c^{in} = 20^\circ\text{C}$ ;  $\delta = 8$  mm;  $L = 0.9$  m).

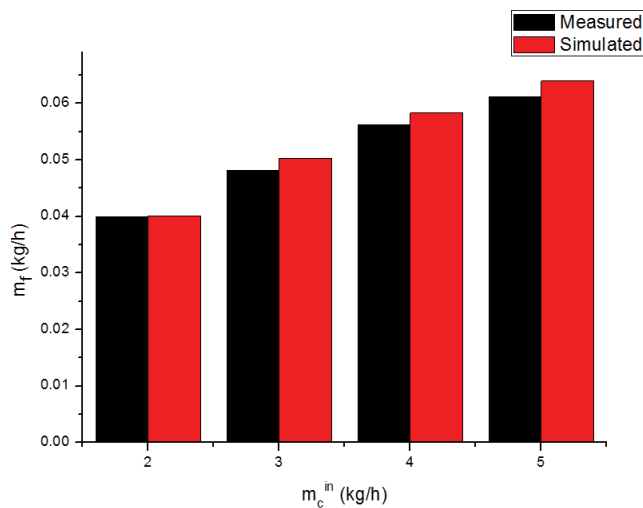


Fig. 16. Effect of the mass flow rate on the freshwater production ( $t_h^{in} = 50^\circ\text{C}$ ;  $t_c^{in} = 20^\circ\text{C}$ ;  $\delta = 8$  mm;  $L = 0.9$  m).

of  $m_f$ . According to the formula of the GOR, the GOR was reduced. The deviations between the calculated and experimental values of the  $m_f$  and the GOR were 10.56% and 3.13%, respectively. The data could then be plotted as shown in Figs. 16 and 17.

#### 5.4. Comparison with other studies

In this study, the water production flux is  $0.937 \text{ kg m}^{-2} \text{ h}^{-1}$ , when the thickness and height of air-gap, inlet temperatures of cold and hot fluid, mass flow rate of cold fluid were 5 mm, 0.9 m,  $20^\circ\text{C}$ ,  $65^\circ\text{C}$  and  $5 \text{ kg h}^{-1}$  respectively. In Cheng et al.'s study [15], they proposed a design of counter current AGMD of the hollow fiber module, when the velocity of cold solution side and hot tube side is  $2 \text{ L min}^{-1}$ , the temperature of the cold solution side is  $20^\circ\text{C}$ , the temperature of the hot tube side is  $80^\circ\text{C}$ , packing density is 0.6, the air-gap thickness is 0.2 mm, the module

length is 0.35 m, the mass vapor flux is  $3.5 \text{ kg m}^{-2} \text{ h}^{-1}$ . Under same mass flow rate of cold fluid, the freshwater production of this paper is about 1.6 time than theirs. Compared with Cheng et al.'s results [15], the value of water production flux in this study is small, but the mass flow rates of AGDD is far less than theirs, the water recovery rate is 3.37% which in Cheng et al.'s study is only 1.42%, and the AGDD operates at atmospheric pressure, the equipment is easy to operate and the material cost is low.

#### 6. Conclusions

- The inlet temperature of the hot flow channel increased, both the freshwater production and the GOR increased. In order to obtain a higher inlet temperature for the hot flow channel, high temperature heat source was required to heat cold fluid ( $t_c^{out}$ ), at the same time, the heat-resistant temperature of the hot flow channel nonmetallic materials for this study should be considered less than  $70^\circ\text{C}$ ; so the device was suitable for a low-grade heat source such as solar energy or industrial waste heat greater than  $70^\circ\text{C}$ , the amount of heating provided by the low-grade heat source was abundant.
- The inlet temperature of the cold liquid was reduced, or the mass flow rate increased; and then the freshwater production increased, but the GOR decreased. If need to ensure the freshwater production and obtain a higher GOR at the same time, then it was necessary to choose the optimal cold liquid inlet temperature and mass flow rate.
- The local heat transfer coefficient decreased as the  $x$  increases, and if the inlet temperature of the cold liquid or the hot liquid increased, the local heat transfer coefficient would increase. The inlet temperature of the hot liquid had a greater influence on the local heat transfer coefficient than the cold liquid. Under the same conditions, the inlet temperature of the hot liquid increased  $10^\circ\text{C}$ , the local heat transfer coefficient increased 42.5% (at  $x = 0$ ); but the inlet temperature of the cold liquid

increased 10°C, the local heat transfer coefficient only increased 6% (at  $x = 0$ ).

### Symbols

$A$	—	Micro-element area, $m^2$
$b$	—	Hot channel width, m
$D_{AB}$	—	Diffusion coefficient of water vapor in air, $m^2 s^{-1}$
$g$	—	Acceleration of gravity, $kg m^{-1} s^{-2}$
GOR	—	Gained output ratio
$H$	—	Enthalpy, $J kg^{-1}$
$h$	—	Heat transfer coefficient, $W m^{-1} K^{-1}$
$J$	—	Diffusion flux, $kg m^{-2} s^{-1}$
$k$	—	Thermal conductivity, $W m^{-1} K^{-1}$
$L$	—	Air-gap height, m
$M$	—	Molar mass, $g mol^{-1}$
$m$	—	Mass flow rate, $kg h^{-1}$
$m_f$	—	Water productive rate, $kg s^{-1}$
$P^i$	—	Partial pressure, Pa
$q$	—	Heat flux, $W m^{-2} s^{-1}$
$R$	—	Universal gas constant, $J mol^{-1} K^{-1}$
$S$	—	Salinity
$T$	—	Temperature, K
$t$	—	Temperature, °C
$y$	—	Mole fraction

### Greek

$\gamma$	—	Latent heat of water evaporation, $J kg^{-1}$
$\delta$	—	Thickness, m
$\varepsilon$	—	Porosity of porous media
$\mu$	—	Dynamic viscosity, Pa s
$\rho$	—	Density, $kg m^{-3}$
$\omega$	—	Solution mass concentration

### Subscript

$a$	—	Air-gap
af	—	Condensate film
ave	—	Average
$c$	—	Cold fluid
cw	—	Cooling plate
fp	—	Between the cold plate and the condensate film
$g$	—	Air
$h$	—	Hot fluid
ha	—	Between the hot channel and the air-gap
$p$	—	Porous
pc	—	Between the cold plate and cold channel
sw	—	Seawater
tm	—	Average heat transfer
tx	—	Local heat transfer
$v$	—	Water vapor
$w$	—	Water

### Superscript

in	—	Inlet
out	—	Outlet

### Acknowledgements

This project is financially supported by the National Natural Science Foundations of China (No. 51876023, No. 51776029).

### References

- [1] Z. Chen, Research on Thermal Solar Water Desalination Technology and System, Chongqing University, Chongqing, 2009.
- [2] C. Chen, Analysis of the Global Seawater Desalination Industry Competition Pattern in 2018-Saudi Arabia's Production Capacity Ranks First in the World, FORWARD-THE ECONOMIST, Shenzhen Foresight Touchplus information Corp., Shenzhen, China, 2018. Available at: <https://www.qianzhan.com/analyst/detail/220/180614-081cc30f.html>, 2018-06-14.
- [3] C. Wang, Characteristics Analysis of Low Temperature Multi-Effect Distillation Seawater Desalination device, North China Electric Power University, Beijing, 2006.
- [4] H. Shao, Application of CFD in Air-Gap Carbon Membrane Distillation Process, Dalian University of Technology, Dalian, 2012.
- [5] H. Geng, H. Wu, P. Li, Study on new air-gap membrane distillation module for desalination, *Desalination*, 334 (2014) 29–38.
- [6] S. Adham, A. Hussain, J.M. Matar, R. Dores, A. Janson, Application of membrane distillation for desalting brines from thermal desalination plants, *Desalination*, 314 (2013) 101–108.
- [7] B.O. Unal, D.Y. Imer, B. Keskinler, I. Koyuncu, Boron removal from geothermal water by air-gap membrane distillation, *Desalination*, 433 (2018) 141–150.
- [8] J.I. Mengual, M. Khayet, M.P. Godino, Heat and mass transfer in vacuum membrane distillation, *Int. J. Heat Mass Transfer*, 47 (2004) 865–875.
- [9] P.A. Hogan, Sudjito, A.G. Fane, G.L. Morrison, Desalination by solar heated membrane distillation, *Desalination*, 8 (1991) 81–90.
- [10] G.T. Zakrzewska, M. Harasimowicz, A.G. Chmielewski, Concentration of radioactive components in liquid low-level radioactive waste by membrane distillation, *J. Membr. Sci.*, 163 (1999) 257–264.
- [11] M. Khayet, A.O. Imdakm, T. Matsuura, Monte Carlo simulation and experimental heat and mass transfer in direct contact membrane distillation, *Int. J. Heat Mass Transfer*, 53 (2010) 1249–1259.
- [12] Ó. Andriessdóttir, C.L. Ong, M. Nabavi, S. Paredes, A.S.G. Khalil, B. Michel, D. Poulikakos, An experimentally optimized model for heat and mass transfer in direct contact membrane distillation, *Int. J. Heat Mass Transfer*, 66 (2013) 855–867.
- [13] S. Huang, M. Yang, J. Tu, Sweeping air membrane distillation: conjugate heat and mass transfer in a hollow fiber membrane tube bank with an in-line arrangement, *Int. J. Heat Mass Transfer*, 108 (2017) 2191–2197.
- [14] S. Cong, X. Liu, F. Guo, Membrane distillation using surface modified multi-layer porous ceramics, *Int. J. Heat Mass Transfer*, 129 (2019) 764–772.
- [15] L. Cheng, P. Wu, J. Chen, Numerical simulation and optimal design of AGMD-based hollow fiber modules for desalination, *Ind. Eng. Chem. Res.*, 48 (2009) 4948–4959.
- [16] D. Singh, K.K. Sirkar, Desalination by air-gap membrane distillation using a two hollow-fiber-set membrane module, *J. Membr. Sci.*, 421–422 (2012) 172–179.
- [17] P. Wang, B. Yu, S. Xu, L. Xu, S. Zhang, L. Li, Study on heat and mass transfer characteristics of AGDD, *Desal. Water Treat.*, 151 (2019) 47–55.
- [18] S. Yang, W. Tao, *Heat Transfer Theory*, Higher Education Press, Beijing, 2006.
- [19] Y. Chou, R.J. Y, The evaporation of a saturated porous layer inside an inclined airflow channel, *Int. J. Heat Fluid Flow*, 28 (2007) 407–417.

- [20] A.S. Alsaadi, N. Ghaffour, J.D. Li, S. Gray, L. Francis, H. Maab, G.L. Amy, Modeling of air-gap membrane distillation-process: a theoretical and experimental study, *J. Membr. Sci.*, 445 (2013) 53–65.
- [21] B. Yu, Study on the Heat Transfer Characteristics of Seawater Desalination in Air-Gap Diffusion Distillation, Dalian University of Technology, Dalian, 2018.
- [22] H. Guo, H.M. Ali, A. Hassanzadeh, Simulation study of flat-sheet air-gap membrane distillation modules coupled with an evaporative crystallizer for zero liquid discharge water desalination, *Appl. Therm. Eng.*, 108 (2016) 486–501.
- [23] M.H. Sharqawy, J.H. Lienhard, S.M. Zubair, Thermophysical properties of seawater: a review of existing correlations and data, *Desal. Water Treat.*, 16 (2010) 354–380.
- [24] M. Jiang, S. Xu, X. Wu, Experimental investigation for heat and mass transfer characteristics of R124-DMAC bubble absorption in a vertical tubular absorber, *Int. J. Heat Mass Transfer*, 108 (2017) 2198–2210.
- [25] C.M. Gijjt, G.W. Meindersma, T. Reith, A.B. de Haan, Air-gap membrane distillation-2 model validation and hollow fibre module performance analysis, *Sep. Purif. Technol.*, 43 (2005) 245–255.
- [26] M.A. El-Rady Abu-Zeid, L. Zhang, W.-Y. Jin, T. Feng, Y. Wu, H.-L. Chen, L. Hou, Improving the performance of the air-gap membrane distillation process by using a supplementary vacuum pump, *Desalination*, 384 (2016) 31–42.